Optical stimulation of cardiac cells with a polymer-supported silicon nanowire matrix

Ramya Parameswaran[a,b,1], Kelliann Koehler[c,1], Menahem Y. Rotenberg[d], Michael J. Burke[c], Jungkil Kim[e,f], Kwang-Yong Jeong[e,f], Barbara Hissa[d,g,h], Michael D. Paul[i], Kiela Moreno[c], Nivedina Sarma[c], Thomas Hayes[c], Edward Sudzilovsky[g], Hong-Gyu Park[e,f,2], and Bozhi Tian[c,d,h,2]

[a]Medical Scientist Training Program, The University of Chicago, Chicago, IL 60637; [b]The Graduate Program in Biophysical Sciences, The University of Chicago, Chicago, IL 60637; [c]Department of Chemistry, The University of Chicago, Chicago, IL 60637; [d]James Franck Institute, The University of Chicago, Chicago, IL 60637; [e]Department of Physics, Korea University, 02841 Seoul, Korea; [f]Korea University (KU)-KIST Graduate School of Converging Science and Technology, Korea University, 02841 Seoul, Korea; [g]Department of Physics, The University of Chicago, Chicago, IL 60637; [h]The Institute for Biophysical Dynamics, The University of Chicago, Chicago, IL 60637; and [i]Program in Molecular Biophysics, Johns Hopkins University, Baltimore, MD 21218

Edited by Charles M. Lieber, Harvard University, Cambridge, MA, and approved November 13, 2018 (received for review September 24, 2018)

Electronic pacemakers can treat electrical conduction disorders in hearts; however, they are invasive, bulky, and linked to increased incidence of infection at the tissue–device interface. Thus, researchers have looked to other more biocompatible methods for cardiac pacing or resynchronization, such as femtosecond infrared light pulsing, optogenetics, and polymer-based cardiac patches integrated with metal electrodes. Here we develop a biocompatible nongenetic approach for the optical modulation of cardiac cells and tissues. We demonstrate that a polymer–silicon nanowire composite mesh can be used to convert fast moving, low-radiance optical inputs into stimulatory signals in target cardiac cells. Our method allows for the stimulation of the cultured cardiomyocytes or ex vivo heart to beat at a higher target frequency.

cardiac | silicon | nanowire | modulation | optical

The electrical conduction system of the heart allows for the coordinated contraction of cardiomyocytes to produce heartbeats. Abnormalities in this system can lead to delayed mechanical activation of specific regions of the heart or pathologically slow heart rates (bradyarrhythmias). Thus, therapies that can either resynchronize the heart or increase the overall beating frequency of the heart are necessary for the treatment of these disorders. Electronic pacemakers are the current standard of care in both cardiac resynchronization therapy and bradyarrhythmias (1). Although these devices are effective in treating these disorders, they are immunogenic and can lead to inflammation and infections at the implantation site, require the use of physical wires that can limit the spatial resolution and location of the treatment, and can foul in the physiological environment of the chest cavity as well as produce unpredictable and unwanted electrochemical reactions at the tissue interface.

Alternatives to pacemaker therapies include the use of optical or mechanical methods to alter the beating frequency of cardiomyocytes (2–11). Optogenetics is one promising optical method that uses light-activatable ion channels to controllably modulate cardiac cell excitability (9). Although effective and noninvasive, optogenetic cardiac modulation could be difficult to implement in vivo and clinically due to the need for gene transfection. Other optical modulation techniques rely on light stimuli alone or the use of a material that can convert the optical input into heat or electricity to alter the membrane voltage of the target cells (2–7). For example, infrared laser inputs can induce contraction of cultured neonatal rat cardiomyocytes and embryonic quail hearts at the same frequency of the laser pulses using high irradiances (2, 6). Additionally, 532-nm picosecond laser stimulation in combination with gold nanoparticles has been used to increase the beating frequency of HL-1 cells and neonatal rat cardiomyocytes via a photothermal mechanism (5). Here we present an alternative to the aforementioned methods that uses a freestanding polymer–silicon nanowire (SiNW) mesh containing a random SiNW network and a moving low-irradiance laser input for optical stimulation of cultured neonatal rat cardiomyocytes and adult rat hearts ex vivo to beat at a target frequency. Target frequencies for stimulation experiments were determined based upon the baseline beating frequency of the dissociated cells or rat hearts, which can especially vary in vitro due to variation in cell concentration and differing batches of neonatal rat offspring. Our stimulation process is one in which target cells are periodically exposed to optical pulse trains until they beat at this applied frequency, instead of a pacing process in which one light pulse immediately results in one cell beat. More specifically, our method allows for an increase in cardiac beating frequency over the course of several low-radiance optical stimulation sessions to a target frequency that is not necessarily phase locked with the optical pulses. The methodology generally consists of (*i*) identifying a prestimulus frequency via imaging or ECG electrodes, (*ii*) optically stimulating cells using a laterally moving laser stimulus with programmed ON/OFF cycles, and (*iii*) tracking a poststimulus frequency as feedback for subsequent stimulation until the cells beat at the target frequency in the case of in vitro cultured cardiomyocytes or tracking cardiac electrical responses during light stimulation via ECG electrodes in the case of an adult heart ex vivo.

Significance

Cardiac conduction disorders are potentially fatal illnesses caused by abnormalities in the heart's electrical conduction system. Current treatments for these disorders, such as pacemakers, are effective but are bulky, rigid, and invasive. Here we develop a method to optically modulate cardiac beating frequency in primary cultured cardiomyocytes and adult rat hearts ex vivo, to a specified target frequency. Specifically, we use a low-irradiance moving laser stimulus and a biocompatible polymer–silicon nanowire composite material to achieve this modulation. This work has implications for future bioelectric studies of the cardiac conduction system as well as therapeutics for cardiac conduction disorders in the clinic.

Author contributions: R.P., K.K., M.Y.R., J.K., K.-Y.J., H.-G.P., and B.T. designed research; R.P., K.K., M.Y.R., M.J.B., J.K., K.-Y.J., B.H., M.D.P., K.M., N.S., T.H., and E.S. performed research; B.H. contributed new reagents/analytic tools; R.P., K.K., M.Y.R., M.J.B., J.K., K.-Y.J., H.-G.P., and B.T. analyzed data; and R.P., K.K., M.Y.R., J.K., H.-G.P., and B.T. wrote the paper.

The authors declare no conflict of interest.

This article is a PNAS Direct Submission.

See Commentary on page 347.

[1]R.P. and K.K. contributed equally to this work.

[2]To whom correspondence may be addressed. Email: hgpark@korea.ac.kr or btian@uchicago.edu.

This article contains supporting information online at www.pnas.org/lookup/suppl/doi:10.1073/pnas.1816428115/-/DCSupplemental.

Published online December 11, 2018.

Polymer–Silicon Nanowire Mesh Characterization

The composite mesh was fabricated using SU-8 (MicroChem) as the polymer support component and coaxial p-type/intrinsic/n-type silicon nanowires (PIN-SiNWs), previously shown to produce photoelectrochemical currents and elicit action potentials in single neurons (12), as the semiconductor modulation component (*SI Appendix*, Fig. S1). With mechanical transfer and subsequent photolithography (Fig. 1*A*), we integrated a high-density mesh of randomly oriented PIN-SiNWs onto an SU-8 grid (Fig. 1*B* and *SI Appendix*, Fig. S1). The resultant composite (SU-8/SiNW) contains a high-density random PIN-SiNW network spanning across the 86 μm × 424 μm window regions in the SU-8 grid (Fig. 1*B* and *SI Appendix*, Fig. S1). Using confocal microscopy, we identified thin filaments of SU-8 polymerized beneath the SiNWs in the window regions (Fig. 1*C*). These thin SU-8 structures were not formed by direct exposure to UV light, because the window regions are blocked by the photolithography mask (Fig. 1*A* and *SI Appendix*, Fig. S2). Moreover, in the absence of SiNWs, we saw no evidence of these thin SU-8 filaments (*SI Appendix*, Figs. S2 and S3), suggesting that the mechanically transferred SiNWs may act as a thermal or optical guide for SU-8 polymerization (Fig. 1*A*).

Optical Stimulation Method for Primary Cardiomyocytes

With this polymer–silicon nanowire mesh, we designed an optical stimulation method for cultured cardiomyocytes (Fig. 2). This approach pairs confocal laser scanning (13) with a PIN-SiNW–enabled waveguiding of the light stimulus to produce a combinatorial collection of transient inputs over whole cell areas (Fig. 2). First, we scanned a diffraction-limited 0.6-μW 514-nm laser spot over a region of interest, at a 1-kHz line scan rate (f_L) with two repeats for each line, resulting in a 50% duty cycle at the stimulation frequency (Fig. 2 *A* and *B* and *SI Appendix*, Fig. S4). We used two repeats to strengthen any possible stimulative effect from the local Si/cell interfaces. Given that each line crosses a total of 1,024 pixels (pixel area, ∼0.09 μm^2), this yields an average pixel scan rate of 1.024 MHz, which is much faster than the frequency range for targeted cardiomyocyte contractions or the stimulation frame rate (∼0.5–2 Hz, f_F). After the full area of interest is scanned (i.e., ON state), an OFF state without laser scanning is employed to match the desired stimulation frame rate (f_F; Fig. 2*D*). Stimulating cells toward f_F is achieved via cycles of ON/OFF modulations (Fig. 2*D*). Each pixel (e.g., the orange square in Fig. 2*B*) experiences six primary incident fluxes per stimulation frame, due to the larger diffraction-limited airy disk diameter (>500 nm) of the laser beam versus the size of a single pixel (303 nm by 303 nm or ∼0.09 μm^2), and the choice of two scanning repeats used in the present study (Fig. 2*C*). Second, in parallel with the scanning modality, the light absorption and correspondingly the subsequent stimulative input from each pixel also vary due to the distribution of SiNWs. We performed finite-element method (FEM) simulations to generate a map of light absorption in regions of the mesh with SiNWs when the laser spot scans across those regions (Fig. 2*E* and *SI Appendix*, Fig. S3). The simulation shows that the SiNWs allow for light propagation into surrounding pixels. Moreover, light propagation to pixels outside of the diffraction-limited spot only occurs at pixels containing SiNW segments (Fig. 2*E* and *SI Appendix*, Fig. S3). The exact configuration of the SiNWs around the illumination spot determines the distribution of absorbed energy at nearby pixels that contain both a cell and SiNW(s). A region of interest (blue dotted box; Fig. 2*E*) will then absorb light energy under both direct laser illumination (Fig. 2*E*, *Bottom Left*) and laser illumination at a nearby pixel (Fig. 2*E*, *Bottom Right*). The variation of the absorbed energy at each pixel during one on period (Fig. 2*D*) would also be large, given the range of the laser spot location (>3,000 μm^2) and the high-density SiNWs; this would provide variable optical input strengths at each pixel. Taken together, the combination of the scanning operation and the SiNW network efficiently utilizes the laser stimulus, by drastically expanding the cellular modulation positions (i.e., as defined by the 1.024-MHz pixel scan rate and the pixel size of ∼0.09 μm^2) and intensities [i.e., through SiNWs-enabled waveguiding (14–16) and the photoelectrochemical effect (12)], while keeping the laser radiance low. Although the waveguiding effect produced by the SiNW network lowers the spatial resolution of the original light stimulus (spot size of ∼500 nm), it would not compromise the ability of the light spot to perform single-cell targeting, because the original spot size is so much smaller than the size of a single cardiomyocyte.

Optically Stimulating Cardiomyocytes to Beat at a Target Frequency

We next employ this optical stimulation method to stimulate cardiomyocytes to beat at a target frequency. We cultured neonatal rat ventricular cardiomyocytes on fibronectin-coated composite meshes and confirmed the substrate biocompatibility via a live/dead viability assay (*SI Appendix*, Fig. S5). Immunofluorescence images demonstrated that cells grown on the mesh aligned with the long axis of the SU-8 grid structure and were well connected via gap junctions (green) (Fig. 3*A*). Scanning electron microscopy imaging confirmed direct contact between the

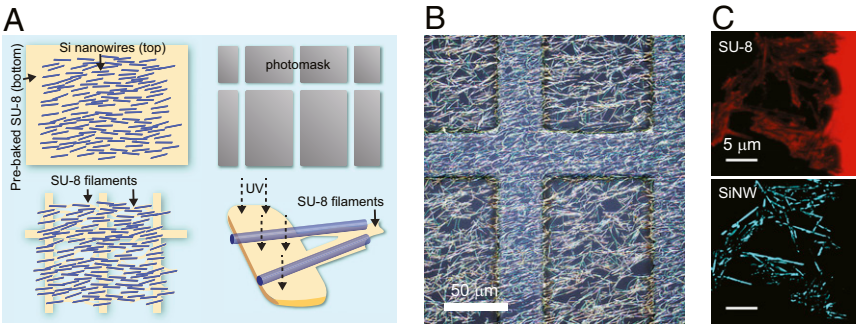

Fig. 1. Freestanding SU-8/PIN-SiNW mesh fabrication for optical stimulation of cardiomyocytes. (*A*) Schematic of fabrication for SU-8/PIN-SiNW mesh. After the SU-8 precursor (yellow) is deposited and prebaked onto a glass slide, SiNWs (blue lines) are deposited into the upper layer of the polymer via mechanical transfer (*Top Left*). Photolithography is performed with a photomask (gray grid structure; *Top Right*) to produce an SU-8 grid structure with interconnected SiNWs (*Bottom Left*). (*B*) Wide-field reflected light microscopy image of an SU-8/PIN-SiNW mesh taken via a CMOS color camera on a 3D confocal laser microscope. (*C*) Confocal microscopy image of SU-8/PIN-SiNW mesh stained with Rhodamine 6G [blue, nanowires (*Bottom*); red, SU-8 (*Top*)], showing position matching between SiNWs and SU-8 filaments.

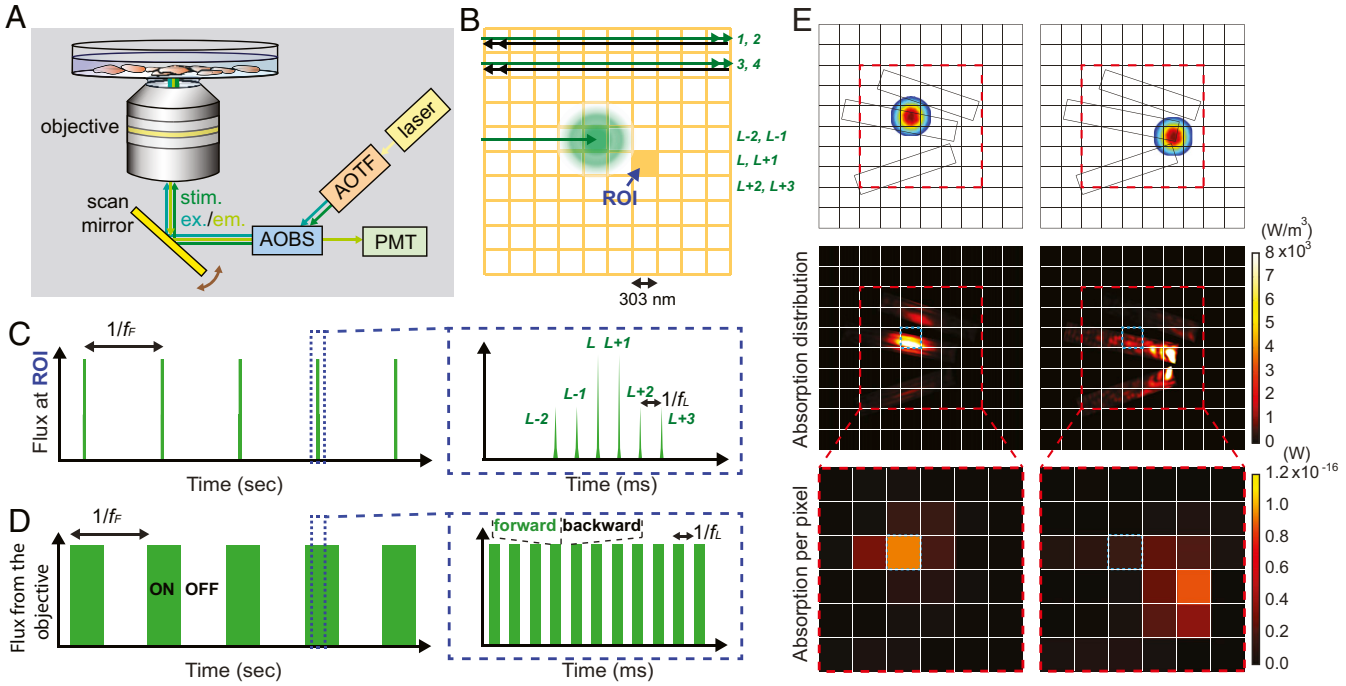

Fig. 2. Fast moving laser scanning pattern developed for stimulation of cultured cardiomyocytes on SU-8/PIN-SiNW mesh. (*A*) Scanning confocal microscopy setup used to optically stimulate primary neonatal cardiomyocytes cultured on a SU-8/PIN-SiNW mesh. The stimulation light (514 nm; green) is focused through a 40× objective lens via a scan mirror (yellow) onto the sample. For recording beating patterns, either DIC imaging or Fluo-4 calcium imaging (shown here) can be used. AOBS, acousto-optical beam splitter (blue); AOTF, acousto-optical tunable filter (orange); PMT, photomultiplier tube. (*B*) Schematic of optical stimulus on a miniaturized pixel grid. The individual pixel size is 303 nm × 303 nm. During optical stimulation, the 514-nm laser (green spot) is scanned line by line at a 1-kHz line scan rate (f_L) with two repeats for each line. Half of the scans for a given line occur in the forward direction (green) and the other half in the backward direction (black). The laser is on when forward (green double-headed arrow, scans 1, 2, 3, and 4) and off when backward (black double-headed arrow). A given pixel, or region of interest (ROI), will experience photon fluxes L − 2 and L − 1 from the pixel above, L and L + 1 at the ROI, and L + 2 and L + 3 from the pixel below as the laser scans. (*C*) Schematic of photon flux (*y* axis) at one given ROI (e.g., the filled orange grid in *B*) over time (*x* axis). f_F is the scanning frame rate or the targeted stimulation frequency. At a single ROI, the flux during a single scanning/stimulation frame would experience two low-intensity (L − 2, L − 1), two high-intensity (L, L + 1), and two low-intensity (L + 2, L + 3) pulses (zoomed-in view in *C*). It is doublet because we used two repeats for each line scan. Additionally, the intensity variation is a result of the fact that the laser beam is an airy disk that expands beyond the pixel size. The time between pulses at the ROI is $1/f_L$, where f_L is the laser line scan rate, i.e., 1 kHz in the present study. (*D*) Schematic of the photon flux directly coming out from the objective (*y* axis) over time (*x* axis). The laser is set to scan over the stimulation area with a period of $1/f_F$. ON and OFF denote laser status during scanning in one stimulation frame. Within the ON period, the laser is turned on only in the forward scan (green bar; the zoomed-in view in *D*) and is off during the backward scan (space between green bars; the zoomed-in view in *D*). Within the OFF period of one frame the laser is off, and no scanning occurs. (*E*) FEM simulation to calculate a map of light absorption in regions with SiNWs in a pixel grid. Three 300-nm-diameter SiNWs are introduced for proof-of-concept demonstration, and two different pump positions are examined (*Top*). The wavelength and spot size of the pump light are set to 514 and 520 nm, respectively. The calculated absorption distribution in each pump position (*Middle*) is used to plot the 6 × 6 digitized absorption matrix (*Bottom*). In *Bottom*, the absorption per pixel is calculated by integrating the absorption distribution in each single pixel with a volume of 303 × 303 × 400 nm^3. We also mark the same pixel as a blue dotted box for a clear comparison of the pump position-dependent absorption.

cardiomyocytes and the PIN-SiNWs both on the SU-8 grid itself and in the window regions of the mesh (Fig. 3*B*).

To characterize the cellular response to optical stimulation, we used either differential interference contrast (DIC) or calcium imaging (Fig. 3*C*) to record the beating frequency (*Methods*). The recordings of the cells were performed before and after each optical stimulation period (green and purple bars at the top of Fig. 3*D*) and were separated by user-defined break times (black bars at the top of Fig. 3*D*). Each stimulation period (pink bars at the top of Fig. 3*D*) includes cycles of ON/OFF modulations (Fig. 2*D*). In a representative experiment, we stimulated a group of 11 cardiomyocytes to beat at a target frequency of 700 mHz (light green line, Fig. 3*C*). Before any stimulations, the cells displayed an incoherent beating pattern with frequencies ranging from 0 to 669 mHz, as shown by calcium imaging traces of a representative cell (Fig. 3*C*). After optical stimulation for a total of four stimulation periods that are separated by 2-min breaks, this cell beat at ∼700 mHz (Fig. 3*C*). We observed that the spread of the frequencies decreased with more optical stimulation and that the frequencies measured trended toward the target frequency of 700 mHz (Fig. 3*D*). The poststimulus frequency is not always the same as the prestimulus frequency for the next stimulation session (Fig. 3*D*). The estimated stimulation laser radiant exposure is ∼1.3 mJ/cm^2 per stimulation frame. We also confirmed that the calcium imaging itself cannot yield a stimulatory effect (*SI Appendix*, Fig. S6), given its high acquisition rate (>5 frames per second) is beyond the range that isolated cardiomyocytes can respond to. This approach can be applied to cardiomyocytes with different initial and targeted frequencies (Fig. 3*E*), but the paths can vary as shown in the two traces from targeted stimulation at 700 mHz most likely due to normal variation in baseline cell beating frequencies, cell density, and cell connectivity in the primary culture (Fig. 3*E*). Additionally, to account for these variations, the conditions for individual stimulations (i.e., duration) can be controlled by the user as a real-time feedback to improve the overall stimulation efficacy; for example, the duration of Stim 2 is 2× that of Stim 1 for a targeted stimulation at 1,000 mHz (Fig. 3*E*). We last also showed that our

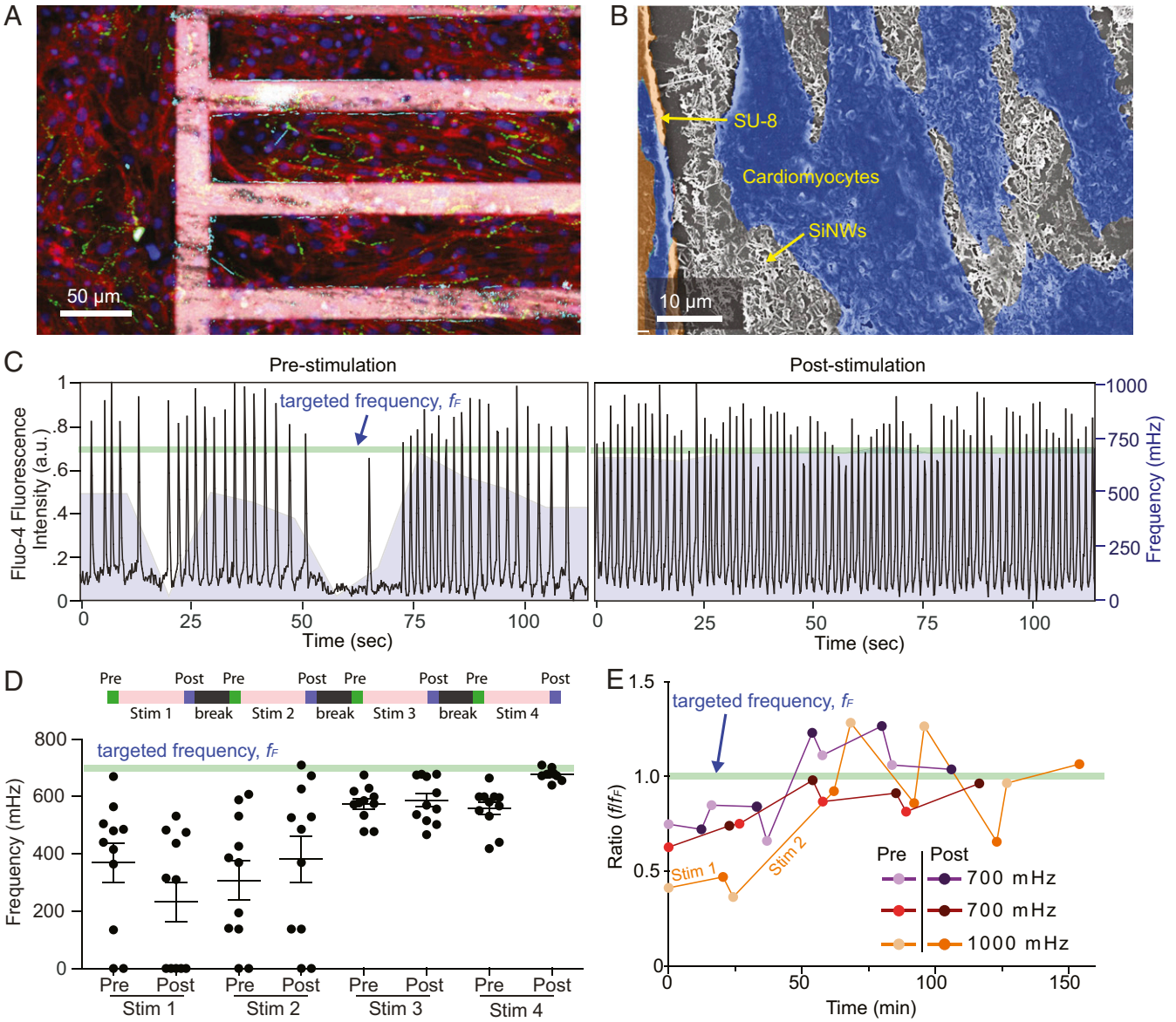

Fig. 3. Optical stimulation of cardiomyocytes with the composite mesh. (*A*) Confocal fluorescence microscope image of primary neonatal cardiomyocytes cultured partly on a fibronectin-coated SU-8/PIN-SiNW mesh (*Right*) and partly on fibronectin-coated glass (*Left*). Mesh was stained with Rhodamine B (pink), and cardiomyocytes were stained with anti-troponin (red), anti-connexin 43 (green), and DAPI (blue). (*B*) False colored scanning electron microscopy image of the biointerface, showing cardiomyocytes (blue), SU-8 grid (orange), and PIN-SiNWs (white). (*C*) Fluo-4 calcium imaging traces (black traces) depicting prestimulation and poststimulation beating patterns for a representative cell, from a group of 11 cardiomyocytes that were stimulated to beat at 700 mHz (light green line). Moving averages of the frequencies of 11 cells (window size is 18 s or 100 imaging frames) were overlaid with the black traces as the purple mountain plots. (*D*) Average frequencies for each stimulation period throughout the stimulation. The stimulation periods were 20.98 (880 frames), 25.64 (1,075 frames), 25.64, and 25.64 min for Stim 1, Stim 2, Stim 3, and Stim 4. Eleven data points (i.e., recorded from 11 cells) are plotted for each prestimulation and poststimulation condition, with their means (black horizontal line) and SEM (black bars above and below average). For all stimulation experiments, length of one particular stimulation period (e.g., Stim 2) was determined based on how the cells responded to the previous stimulation period (e.g., Stim 1). (*E*) Average beating frequencies were plotted as ratios of the beating frequency to the targeted beating frequency (or the scanning frame rate, f_F) over time for cells from three different stimulation experiments. Four cells were used in the 700-mHz experiment (purple), five cells in the second 700-mHz experiment (red), and seven cells in the 1,000-mHz experiment (orange). The frequencies of prestimulation and poststimulation are depicted with lighter colored dots (prestimulation) and darker colored dots (poststimulation). Time between prestimulation and poststimulation measurements includes that used for the prestimulation frequency measurement and the stimulation time. Time between the poststimulation and next prestimulation measurements includes that used for the recording of the poststimulation frequency and the 2-min break time. The green line indicates the targeted frequency (f_F). Connections between dots do not represent real data and are included as a way to guide the trend. These are representative traces of $n = 9$ experiments (91 cells total).

optical stimulation method induces minimum cytotoxicity in the target cells using a live/dead assay (*SI Appendix*, Fig. S5).

Control samples that were cultured on either glass or SU-8 grid meshes with intrinsic Si core-shell nanowires (SU-8/III-SiNW), which have previously been demonstrated to lack a significant photoelectric response (17, 18), did not display behavior which stimulated cells to beat at the target frequency (*SI Appendix*, Fig. S7). Nonscanning stimulation (i.e., wide-field optical illumination with a spot size of ∼1.4 mm) from SU-8/PIN-SiNW meshes can stimulate neighboring cells toward the target

frequency (*SI Appendix*, Fig. S7) using a significantly higher laser radiant exposure (~44 mJ/cm^2 per pulse) but at the expense of light-induced cytotoxicity in the area exposed to light. These results demonstrate that both the high-density random network of PIN-SiNWs and the scanning stimulus are essential to the efficacy of the observed stimulation behavior.

We last also wanted to further characterize the stimulating behavior we observed by studying the importance of the break time (i.e., black bars at the top of Fig. 3*D*) between stimulation periods and how long the cultured cardiomyocytes could maintain their beating frequency after the light stimulus was removed. We found that when we lengthened the break time to 10 min, we could no longer stimulate the target cells (*SI Appendix*, Fig. S8). This suggests that longer break times may prevent the target cells from "remembering" their last optical stimulation period. We also observed that cultured cardiomyocytes can beat at their stimulated frequency for up to 40 min after the optical stimulation is complete (*SI Appendix*, Fig. S8).

Optical Stimulation of Isolated Hearts

We then tested our optical stimulation method in adult rat hearts ex vivo using a Langendorff setup (Fig. 4*A*). The epicardia of the hearts were removed in the left ventricle, and a SU-8/PIN-SiNW mesh was placed onto the exposed myocardium (Fig. 4*A*). The mesh conformably wraps around and adheres to the wet curved surface of the myocardial tissue via capillary action without the need for sutures or tissue adhesives (Fig. 4*A*). Contact angle experiments suggest that this observed phenomenon occurs as a result of increased water adhesion to both the SU-8 microstructure and the SiNWs in the mesh (*SI Appendix*, Fig. S9).

In isolated hearts, unlike in cultured cells (Figs. 2 and 3), the fast-moving illumination interface was made possible by constant change of the sample locations due to the mechanical beating motion of hearts. A 532-nm laser (19.7 mW) was focused through a 5× objective onto the SU-8/PIN-SiNW mesh on the heart and was set to pulse at the target frequency via a waveform generator with a 20% duty cycle (Fig. 4*A*). The frequency of the

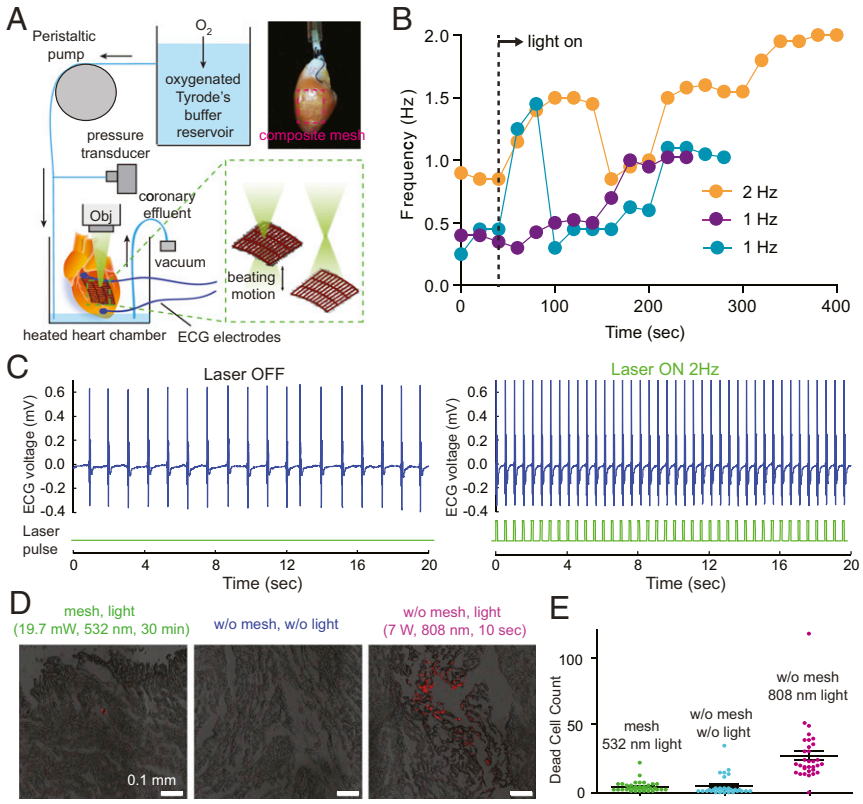

Fig. 4. Optical stimulation of isolated adult hearts. (*A*) Langendorff setup used to assess optical stimulation of adult rat hearts. Oxygenated Tyrode's buffer reservoir was perfused into the aorta of an adult rat heart in a chamber maintained at 37 °C, and the perfusion rate of the buffer was controlled by a peristaltic pump. ECG electrodes were placed on the apex and aorta, and both the perfusion pressure, which was transduced to a recordable signal through a transducer, and the ECG recordings were connected to an amplifier that was interfaced with a computer. A 532-nm laser was focused through a 5× objective around the SU-8/PIN-SiNW mesh (red dashed box in the top right image) placed onto exposed myocardium on the left ventricle without the use of adhesives or sutures. The movement of heart during beating yielded ~0.2 mm location variation of the mesh. (*B*) Beating frequencies of three different adult hearts, 40 s before being exposed to 532 nm laser light (first two points of each trace) and during exposure to 532 nm laser light (all other points in the traces). Dashed line indicates the time when laser is on. Connections between dots do not represent real data and are just a way to guide the trend. (*C*) Electrocardiogram recordings from an adult heart with a SU-8/PIN-SiNW mesh, before (*Left*) and during (*Right*) stimulation with 532-nm laser pulses at 2 Hz on the SU-8/PIN-SiNW mesh. Light pulses are indicated in green under the ECG traces (blue). This is a representative trace from $n = 5$ different hearts and $n = 5$ different experiments. (*D*) Assessment of phototoxic effects of laser stimulation of adult rat hearts. Adult rat hearts with SU-8/PIN-SiNW meshes pulsed with laser for 30 min at 3.5 Hz (19.7 mW, 532 nm), adult rat hearts alone without any optical stimulation, and adult hearts pulsed for 10 s at 3.5 Hz (7 W, 808 nm) laser to intentionally induce phototoxicity. Dead cells were stained with propidium iodide. Cryosectioning of 5-μm heart slices to a depth of 750 μm was performed, and confocal imaging of the slices (DIC) is shown (red indicates dead cells). These images are representative of three different experiments for the mesh, four experiments for the heart alone, and five experiments for the infrared (IR) laser condition. (*E*) Dead cells were counted using the ImageJ particle counting macro from two different heart experiments with 34 slices, two different heart experiments with 32 slices, and two different heart experiments with 32 slices for the SU-8/PIN-SiNW mesh, heart alone, and IR laser conditions, respectively. Each point on the graph represents one dead cell count from one slice. Means and SE are indicated on the graph with a black horizontal line and black bars above and below the average, respectively.

beating heart was recorded via ECG electrodes that were placed on the apex and aorta of the heart. The fast variation in the laser spot location and intensity due to the contractile heart beating motion, as well as the intensity modulation from SiNW-enabled waveguiding, yielded an analogous situation to the aforementioned scanning laser stimulus (Figs. 2 and 3). However, in this case, the scanning occurs due to the focus change, causing variations in optical stimulus intensities and locations hitting the heart (Fig. 4*A*). Additionally, in this case, we do not employ break times in the laser stimulation approach and measure the heart's response during the application of optical stimulus, not after due to the ease with which we can use ECG electrodes simultaneously with the optical stimulus.

We then assessed the efficacy of stimulating hearts through optical stimulation of SU-8/SiNW mesh-covered hearts. We demonstrate that stimulating hearts at a specific frequency using SU-8/PIN-SiNW meshes will direct hearts to beat at various target frequencies (Fig. 4*B*). We found that the path to the target frequency was characterized not by a steady increase in frequency over time but by a series of slight rises and falls in frequency. The stimulation ended in the target frequency over the span of ∼4–7 min of light exposure (Fig. 4*B*). Representative results show stimulation of one heart from a baseline of 0.9 Hz to the targeted 2 Hz after 5 min of 532-nm pulsed light exposure (Fig. 4*C*). When we attempted to stimulate hearts using SU-8/III-SiNW meshes or light alone, we observed no successful increase in beating frequency to the target frequency within a 6-min span of optical illumination (*SI Appendix*, Fig. S10), suggesting dopant modulation in nanowires is critical. These results demonstrate an easily implemented optical stimulation method for hearts ex vivo.

Last, we assessed cytotoxicity in hearts exposed to the pulsed light stimulus for 30 min using propidium iodide (Fig. 4*D*). We found that SU-8/PIN-SiNW mesh-covered hearts pulsed with 532-nm light at 3.5 Hz had an average of 4.17 ± 0.64 dead cells in a 1-mm^2 area in 34 heart slices in the region exposed to light, compared with 4.41 ± 1.26 dead cells in a 1-mm^2 area in 32 control slices with no light exposure for 30 min. As a positive control for the dye, we exposed hearts to 7 W of 808-nm laser light pulsed at 3.5 Hz for 10 s and induced visible tissue death with an average of 26.06 ± 3.4 dead cells in a 0.68-mm^2 area in 32 heart slices in the region exposed to light. These results indicate that optical stimulation of the SU-8/PIN-SiNW mesh does not induce significant cytotoxicity in adult rat hearts.

Outlook

In summary, we have developed a flexible polymer–silicon nanowire mesh containing a random network of PIN-SiNWs for the optical stimulation of cultured primary cardiomyocytes as well as adult hearts ex vivo (Fig. 1*A*). This stimulation approach is characterized by fast variation of both the optical stimulation intensity and position, yielding high modulation efficiency and a low radiance requirement. Our method also allows for the stimulation of both groups of cells and tissue to a specified target frequency in a minimally invasive manner, lacking the requirement of bulky physical electrodes and causing little to no cytotoxicity in the region exposed to light. Although we do not know the exact biological adaptation mechanisms that the cells are employing to result in the observed increases in beating frequencies, we hypothesize that the mechanisms would be similar to those of other electrical pacing methods. Thus, adaptations that are normally seen during electrical pacing, such as gap junction remodeling (increased expression of connexins, such as connexin-43 gap junctions), cardiac hypertrophy, and increased contractile apparatus development (aligned striations and higher troponin expression), could be occurring during the optical stimulation. Limitations of our study include the need for a light stimulus that may not be able to penetrate the chest cavity. However, due to the fact that silicon absorbs in the near-infrared (NIR) wavelength regime, NIR light stimuli could be utilized to penetrate tissue more easily. Using an implantable micro-LED as an alternative approach would also be much less bulky and immunogenic than traditional pacemaker devices and would be advantageous for addressing the optical penetration issue. This approach would additionally be compatible with the need for longer-duration optical stimulations in a clinical setting due to limitations in the stimulation lifetime of our method. Our findings have implications for both fundamental biointerface studies (19–24) and photoresponsive cardiac therapeutics in the clinic.

Methods

Nanowire Synthesis. Coaxial PIN-SiNWs were synthesized as previously described by Parameswaran et al. (12) using a gold (Au) nanocluster-catalyzed chemical vapor deposition (CVD) process. During the nanowire growth, silane (SiH_4) was used as the Si reactant, diborane (B_2H_6, 100 ppm in H_2) as the p-type dopant, phosphine (PH_3, 1,000 ppm in H_2) as the n-type dopant, and hydrogen (H_2) as the carrier gas. For the p-type core nanowire growth, SiH_4, B_2H_6, and H_2 were delivered at flow rates of 2, 10, and 60 standard cubic centimeters per minute (sccm), respectively. For the intrinsic Si shell (i-shell) deposition, SiH_4 and H_2 were delivered at 0.3 and 60 sccm, respectively. Flow of PH_3 gas was then added for the n-type outer shell deposition at a flow rate of 1.5 sccm. The core growth was carried out at 470 °C at a pressure of 40 torr for 30 min. Before i-shell deposition, growth was paused in a vacuum for 20 min until the CVD furnace temperature was stabilized at 750 °C in preparation for shell deposition. The shell depositions were performed at 750 °C at a pressure of 20 torr for 15 min per shell.

Coaxial intrinsic/intrinsic/intrinsic-SiNWs (III-SiNWs), consisting of intrinsic Si cores and intrinsic Si shells, were synthesized using the same growth process as that of PIN-SiNWs, except with only silane and hydrogen carrier gas, and 30 min growth time for core growth and 30 min for shell deposition.

SU-8/SiNW Mesh Fabrication. SU-8 structures were fabricated using SU-8 2005 (MicroChem) permanent epoxy negative photoresist via photolithographic patterning. SU-8 precursor was deposited onto IPA and acetone-cleaned glass coverslips via a two-step spin coating (Laurell WS-650 Spin Coater) protocol: (*i*) 5 s at 2,500 RPM and (*ii*) 55 s at 150 × *g*. Samples were prebaked at 65 °C for 180 s and 95 °C for 180 s PIN-SiNWs or III-SiNWs attached to their growth substrate were cleaned in a 10% HF solution for 90 s, rinsed in DiH20, and dried under N_2 (g) in order remove the oxide layer. SiNWs were subsequently integrated into the prebaked SU-8 precursor via mechanical translation. During mechanical translation, SiNW wafers were laid atop the SU-8 surface such that the SiNWs and SU-8 precursor were in direct contact and translated with light pressure across the surface. An EVG 620 semi-automatic double side mask aligner was used to photolithographically pattern samples using a quartz mask fabricated at Argonne National Laboratories with various grid patterns and 365-nm UV light source at a 175-mJ exposure dose. A postexposure bake of the sample was subsequently performed at 65 °C for 180 s and 95 °C for 180 s. Samples were developed in SU-8 developer solution (MicroChem SU-8 Developer) for 30 s and rinsed in isopropyl alcohol (IPA) for 15 s. A final postbake was then performed at 165 °C for 20 min. Quality of two samples from each batch was assessed by a profilometer (Bruker Dektak XT-S Profilometer) to check that the height of the resultant SU-8/SiNW mesh was in fact 5 μm and that the mesh sidewalls were intact.

Drop Shape Analysis. SU-8/PIN-SiNW meshes, SU-8 meshes, and SU-8 sheets were first lifted off of the glass slides they were fabricated on by wet chemical etching with a 48% Hydrofluoric acid (HF) [Fluka Chemical Abstracts Service (CAS) no. 7664-39-3] solution for 20 s at room temperature. SU-8-structures were rinsed six times in 3 mL of DI water to remove all of the HF from solution. Samples were deposited onto acrylic scaffolds with a laser-cut 6-cm-diameter hole. Samples were then positioned above the hole and were loaded onto the drop shape analyzer (Kruss DSA100). Sessile drops of 2–3 μL were formed on the DSA needle above the SU-8 structures. Drops were brought into contact with the samples, and the needle was pulled away to leave the drop on the surface of the sample. Contact angles were measured via the sessile drop method. At least 10 samples were measured from different synthesis batches to ensure consistency. Droplet pinning was analyzed by recording a video of the drying process of 2–3 μL sessile drops and

tracking the contact angle and drop diameter to identify water pinning during droplet evaporation for each sample.

SU-8/SiNW Mesh Preparation for Cardiomyocyte Culture. SU-8/SiNW meshes were adhered to glass bottom Petri dishes for cell culture. The glass surfaces were functionalized with (3-Aminopropyl) triethoxysilane (APTES) (Sigma-Aldrich CAS no. 919-30-2), followed by chemical crosslinking to the epoxy groups of SU-8. Briefly, glass bottom Petri dishes (35-mm Glass bottom dish with 20-mm microwell no. 1 cover glass no. D35-20-1-N; Cellvis) were plasma cleaned for 2 min (100 W). Plasma-cleaned glass bottom dishes were coated with 1 mL APTES [(3-Aminopropyl) triethoxysilane] (Sigma Aldrich CAS no. 13822-56-5) for 2 min to functionalize the surface. SU-8/SiNW mesh samples were lifted off via the process described above for DSA measurements and transferred to functionalized dishes with the SiNWs oriented upward. Chemical crosslinking of SU-8/SiNW meshes to APTES was achieved by heating dishes to 80 °C, with a 5.5-g weight pressing the SU-8/SiNW mesh into the glass surface. SU-8 meshes in glass bottom culture dishes were sterilized under UV light for 24 h and coated with human plasma fibronectin at a concentration of 0.5 mg/mL (Thermo Fisher CAS no. 33016015) for 2 h at 37 °C before being used for cell culture.

Cell Culture Protocol. Hearts were excised from P1 neonatal rats into HBSS without Ca^{2+} or Mg^{2+} (Fisher Scientific 14-175-145) on ice and washed six times to eliminate red blood cells. Atria were subsequently removed from each heart, and remaining ventricles were minced into three to four pieces. Ventricles were incubated on a shaker overnight at 4 °C in a 0.05 mg/mL trypsin solution (Worthington Biochemical TRL3 LS003708) in HBSS (Gibco 14175-079). They were then transferred to a 37 °C water bath, and the activity of the trypsin enzyme was inhibited with a 2 mg/mL soybean trypsin inhibitor solution in HBSS. Hearts were then further digested in 1 mg/mL collagenase type II (0.22 μm filtered) (Worthington Biochemical CAS no. LS004202) in L15 medium (Thermo Fisher 11415064) for 45 min in a 37 °C water bath with manual shaking every 5 min. Gentle mechanical trituration of the digested hearts was next performed with a plastic pipette 10 times in a tissue culture hood. The resulting cells were passed through a 70-μm filter and incubated at room temperature for 30 min. Cells were then resuspended into cardiac culture medium (DMEM + 10% FBS + 100 U/mL penicillin + 100 μg/mL streptomycin) (FBS, Gibco Thermo Fisher 10437028; Penicillin-streptomycin, Thermo Fisher Scientific 10378016). Cells were then plated onto 10-cm tissue culture treated Petri dishes in a 37 °C 5% CO_2 incubator for 2 h to exclude excess smooth muscle cells and fibroblasts from the cardiomyocyte culture. Cardiomyocytes from the supernatant were then plated at a concentration of 500,000 cells per dish onto fibronectin-coated SU-8/PIN-SiNW meshes on glass bottom Petri dishes. All animal procedures were conducted in complete compliance with and approval from the University of Chicago Institutional Animal Care and Use Committee (IACUC) Animal Care and Use Protocol.

Scanning Electron Microscopy. Cardiomyocytes were cultured onto the fibronectin-coated SU-8/PIN-SiNW meshes for 48 h, and the media was changed at the 24-h time point after seeding. Cultures were subsequently fixed with 4% paraformaldehyde (Sigma-Aldrich CAS no. 30525-89-4) and stained with 1% osmium tetroxide (Sigma CAS no. 20816-12-0) for 1 h at room temperature. The samples were then dehydrated with increasing concentrations of ethanol and subsequently critical point dried before being sputter-coated with 8 nm of Platinum/Palladium metal. Images were taken on a Carl Zeiss Merlin FEI-SEM.

Immunofluorescence. SU-8/PIN-SiNW meshes were made with SU-8 precursor solution containing ~0.1 mg/mL Rhodamine B (Sigma Aldrich CAS no. 81-88-9). Cardiomyocytes were cultured onto fibronectin-coated Rhodamine B SU-8/PIN-SiNW meshes on glass bottom Petri dishes. After 3 d of culture, cells were fixed with 4% paraformaldehyde for 10 min, permeabilized with 0.2% Triton-X (Fisher Scientific CAS no. 9002-93-1) solution for 5 min, and blocked for an hour with 3% BSA (Fisher Scientific CAS no. 9048-46-8) solution. Samples were then stained with anti-cardiac Troponin I primary antibody (Abcam ab47003) (1/400 in 3% BSA) and anti-Connexin 43 primary antibody (Millipore Sigma MAB3067) (1/100 in 3% BSA) overnight at 4 °C. Cells were subsequently stained for 1 h with AlexaFluor 594 goat anti-rabbit IgG secondary antibody (Molecular Probes no. A11037) and AlexaFluor 488 goat anti-mouse IgG secondary antibody (Molecular Probes no. A1101) in the dark for 1 h at room temperature. Last, cells were stained with DAPI (Sigma Aldrich CAS no. 28718-90-3) at room temperature for 5 min. Samples were visualized (cardiomyocytes on SU-8/PIN-SiNW mesh and neighboring cardiomyocytes on glass) on the Caliber I.D Confocal Scanning microscope using a 20× (NA 0.5) objective. DAPI signal was recorded by a 405-nm laser, cardiac Troponin I staining by a 640-nm laser, Rhodamine 6G signal by a 561-nm laser, Connexin-43 staining by a 488-nm laser, and SiNWs in scattering mode with the 785-nm laser.

Cell Viability Assay. Cardiomyocytes cultured on either fibronectin-coated glass bottom Petri dishes alone or glass bottom Petri dishes with fibronectin-coated SU-8/PIN-SiNW meshes were stained, after 3 d of culture, with a live/dead cell viability assay kit (Thermo Fisher Scientific no. L3224). Cells were imaged after staining for 45 min on the Leica SP5 confocal microscope with a 40× objective. A 488-nm laser was used to visualize the live stain, and 514-nm laser was used to visualize the dead stain. The numbers of live cells in culture on the mesh or on glass were counted visually. Cardiomyocytes optically stimulated on the SP5 confocal system for a total of 75 min were also stained for viability on either glass or the SU-8/PIN-SiNW mesh.

Optical Stimulation of Cardiomyocytes. Cardiomyocytes cultured for 3 or 4 d were stimulated to beat at a target beating frequency using a Leica SP5 Laser Scanning Confocal Microscope. Cells cultured atop a fibronectin-coated glass bottom Petri dish, SU-8/PIN-SiNW mesh, or SU-8/III-SiNW mesh were stained with Fluo-4 AM intracellular calcium dye (Fluo-4, AM, cell permeant Thermo Fisher no. F14201) at a concentration of 0.1 μg/μL for 20 min at 37 °C. Cells were subsequently washed twice in modified Tyrode's buffer (NaCl 132 mM, KCl 4 mM, $MgCl_2$ 1.2 mM, $CaCl_2$ 1.8 mM, Hepes 10 mM, glucose 5.5 mM, pH 7.4). Cells were then kept in 3 mL of modified Tyrode's buffer at 37 °C incubator on the microscope stage for the duration of the experiments. The Argon laser line used for both recording and stimulation (i.e., stimulation) was set to 30% of the maximum power. Prestimulation cellular beating frequency was recorded via a 40× objective (NA 1.3) by a 488-nm laser to monitor Fluo-4 calcium flux before stimulation. The images were recorded at a frame frequency of 5.6 Hz. Alternatively, differential interference contrast (DIC) imaging can be used to monitor the beating frequency. Once the prestimulation frequency was calculated, the target beating frequency was set using the following criteria: (*i*) if the prestimulation beating frequency was consistent, then it must be lower than the target frequency (usually ~30–60% of the target frequency) and (*ii*) if the prestimulation beating frequency was inconsistent, then the highest beating frequency in any given time interval must be lower than the target frequency. As an example, the stimulation pattern for optically stimulating cells to beat at a target frequency of 700 mHz will be described here. The target frequency was achieved via a series of ON/OFF cycles (see Fig. 2 and *SI Appendix*, Fig. S4 for the definition of ON and OFF). During stimulation, the 514-nm laser (Argon ion air cooled continuous wave laser) was rastered at a frequency of 1,000 Hz (line scan rate) over the entire stimulation area (512 × 350 pixels) line by line. The line repeat was set to 2 with unidirectional scanning. The measured power out of the 40× objective of the stimulation laser is 0.615 μW, and the optical stimulation radiant exposure for each frame is ~1.3 mJ/cm^2. The stimulation durations in individual stimulation periods ranged from 10 to 35 min. This range of stimulation period durations was determined based upon the initial experiments, which demonstrated that stimulation periods shorter than 7 min were not long enough to produce a noticeable increase in beating frequency, and durations longer than 35 min resulted in decrease in cell health (i.e., break times are necessary). After stimulation, a poststimulation cellular beating frequency was determined by Fluo-4 calcium imaging in the same manner as the prestimulation recordings. Samples were then allowed to break for a defined period (e.g., 2 or 10 min). The full cycle (prestimulation recording, stimulation, and poststimulation recording, break) was repeated four to five times, resulting in total stimulation times of 57–127 min. Variation in the number of cycles or total stimulation time to reach the target frequency was due to physiological variation in the cardiomyocyte cultures from one isolation to the next. Additionally, during a given experiment, the length of each stimulation period duration was determined by assessing the poststimulation beating frequency from the previous period (i.e., user feedback). For experiments assessing the effects of break time (Fig. 3*F*) between stimulation cycles, cardiomyocytes were not stained with Fluo-4 and instead recorded via DIC imaging.

Analysis of Cardiomyocyte Beating Frequency. For all experiments in which cardiomyocytes were stained with Fluo-4 calcium dye, calcium oscillations, as measured by changes in Fluo-4 fluorescence intensity over a 107.8-s (600-frame) time period before and after optical stimulation periods (i.e., prestimulation and poststimulation measurements), from individual cells were normalized and plotted (raw traces). They were further analyzed with a fast Fourier transform in Python according to the protocol outlined by Uhlén (25)

in 2004. The resultant frequencies calculated by the Fourier transform algorithm were plotted as a moving average, with a series of average frequencies calculated over 18-s subsets of data over the 107.8-s prestimulation and poststimulation time periods as in Fig. 3 *E*–*G*. The moving average was used to calculate the spread of the frequencies over the full 107.8 s as opposed to one frequency calculation for the full 107.8 s to get a more accurate calculation over that time period. Moving Fourier Transforms were performed and displayed as mountain plots (Fig. 3*C*) by applying a Fourier transform over a window of 100 points (18 s) with the returned frequency value plotted at the center of the window. The Fourier transform window is then shifted 50 points and calculated again resulting in a point plotted every 9 s on the mountain plot. All frequencies from each 18-s window for a single cell within a given prestimulation or poststimulation recording period were also plotted as individual points in Fig. 3*D*. For all experiments in which cardiomyocyte beating was recorded via DIC imaging, we determined beating frequencies by watching the recorded videos of the beating cells and counting the number of contractions each cell experienced during the duration of the video.

Nonscanning Optical Stimulation of Cardiomyocytes with SU-8/PIN-SiNW Mesh. Cardiomyocytes cultured for 3 or 4 d atop a fibronectin-coated SU-8/PIN-SiNW mesh were stained with Fluo-4 AM intracellular calcium dye (Fluo-4, AM, cell permeant Thermo Fisher no. F14201) at a concentration of 0.1 μg/μL for 20 min at 37 °C. Cells were subsequently washed twice in modified Tyrode's buffer (NaCl 132 mM, KCl 4 mM, $MgCl_2$ 1.2 mM, $CaCl_2$ 1.8 mM, Hepes 10 mM, glucose 5.5 mM, pH 7.4). Cells were then kept in 3 mL of modified Tyrode's buffer at room temperature on the microscope stage for the duration of the experiments. Beating frequency was measured via a GFP fluorescence filter cube to monitor oscillations in Fluo-4 AM dye fluorescence on an Olympus BX-UCB upright microscope and Hamamatsu EM-CCD digital camera. Cardiomyocytes were stimulated to beat at a target beating frequency using a 532-nm DPSS laser (LaserGlow), not focused through an objective (spot size, 1.4 mm), at a power of 3.33 mW pulsing at the target beating frequency with a duty cycle of 20%. The radiant exposure of the laser stimulus was ∼44 mJ/cm^2 per pulse. To assess changes in beating frequency due to the optical stimulus, calcium imaging measurements were taken before and after optical stimulation (i.e., prestimulation and poststimulation measurements). Cells in various regions within a 4-mm radius were optically stimulated for total durations of 7, 12, or 30 min before recording a poststimulation frequency.

Ex Vivo Cardiomyocyte Stimulation with SU-8/SiNW Mesh. Adult rats were heparinized (1,000 IU/kg IP) and anesthetized using open-drop exposure of isoflurane in a bell jar configuration. Hearts were removed and placed in ice cold HBSS buffer, and the aortas were cannulated in preparation for use in a Langendorff setup. Oxygenated Hepes-buffered Tyrode's solution (containing, in mM, NaCl 126, KCl 5.4, Glucose 10, Hepes 10, $MgCl_2$ 1, $CaCl_2$ 2, $MgSO_4$ 1.2, NaH_2PO_4 0.39; bubbled with 99.5% O_2; pH titered to 7.3 by 2M NaOH) was perfused through the cannulated aortas. The perfusion was passed through a heating coil and bubble trap (Radnoti), and the hearts were placed in a water-jacketed beaker (Fisher Scientific) to maintain the temperature at 37 °C. The perfusion rate was controlled by a peristaltic pump to obtain perfusion pressures of 80–100 mm Hg (∼10–15 mL/min), which were monitored using a BP-100 probe (iWorx). For ECG recordings, needle electrodes were positioned on the apex and aorta and connected to a C-ISO-256 preamplifier (iWorx). Both recordings (ECG and perfusion pressure) were amplified using an IA-400D amplifier (iWorx) and interfaced with a PC using a DigiData 1550 digitizer with pClamp software (Molecular Devices). To lower the heart rate, the atria were removed. To allow for direct interaction of the SU-8/PIN-SiNW or SU-8/III-SiNW with the cardiomyocytes, a small portion (∼20 mm^2) of the myocardium was exposed by removing the epicardium using a scalpel. SU-8/PIN-SiNW or SU-8/III-SiNW meshes were lifted off glass slides, as previously described, and were deposited onto clean glass slides in a thin film of water with the SiNWs oriented upward. These glass slides were brought into light contact with the exposed myocardium, allowing for the SU-8 structures to wrap around and stick to the heart via capillary adhesion; this transfer process ensures direct contact between the SiNWs and cardiomyocytes. Hearts were then stimulated to beat at a target frequency by focusing a 532-nm laser through a 5×/0.10 Olympus UIS 2 MPlanN objective onto the SU-8/SiNW mesh. A waveform generator was used to adjust the frequency of the laser pulses to the intended target frequency with a 20% duty cycle. ECG recordings were used to assess beating frequency of the hearts before and during optical stimulation. All animal procedures were conducted in complete compliance with and approval from the University of Chicago IACUC Animal Care and Use Protocol.

Phototoxicity of Heart Slices. Adult rat hearts were set up on a Langendorff perfusion system as described above. Hearts with SU-8/PIN-SiNW meshes were optically stimulated for 30 min with a 532-nm laser at 19.7-mW power at a frequency of 3.5 Hz and a 20% duty cycle. Control samples were prepared in the same way (with removed epicardia but no mesh) and were either not exposed to laser light for 30 min or exposed to 10 s of 3.5-Hz (20% duty cycle) pulsed infrared (808-nm) laser light at 7 W to induce visible cell death. All hearts were perfused with 30 μM propidium iodide (PI) solution for 20 min, as in Jenkins et al. (11), to stain for dead cells. Hearts were subsequently washed with Tyrode's buffer for 40 min and placed into ice cold Tyrode's buffer. The regions of light exposure on the hearts were excised with scissors and embedded in Tissue-Tek O.C.T. (Sakura Finetek from VWR, cat. no. 25608-930). The embedded tissue was then frozen in a 2-methylbutane dry ice bath and stored at −80 °C. Tissue was cryosectioned in 5-μm sections, collected every 50 (SU-8/PIN-SiNW mesh) or 100 μm (SU-8/PIN-SiNW mesh, control sample, infrared sample) to a total depth of 750 μm. Tissue sections were visualized on a Leica SP8 confocal microscope using a 10× objective (NA 0.4 dry) and a 561-nm laser line. Quantification of cell death was performed in ImageJ with a particle-counting macro.

Finite-Element Method Optical Simulations. The 3D FEM was used to calculate light absorption in SiNWs. The simulation domain was digitized by 10 × 10 pixels in which 1 pixel had a size of 303 × 303 nm^2. The horizontally polarized Gaussian beam with a wavelength of 514 nm, a spot size of 520 nm, and an electric field of 1 V/m was incident to the center of a single pixel and scanned across the domain. The diameter of a SiNW was set to 300 nm, and the surrounding area was made to be water (refractive index is 1.33). Then, the absorption distribution was calculated by 1/2 **J**·**E***, where **J** and **E** are the polarization current density and electric field, respectively. The refractive index and extinction coefficient of bulk Si at 514 nm were used in the calculation. In addition, by integrating the absorption distribution in each pixel (with a height of 400 nm), we plotted the 6 × 6 absorption matrix (absorption per pixel).

ACKNOWLEDGMENTS. We thank The University of Chicago Integrated Light Microscopy Core Facility, especially Dr. Christine Labno, for their resources and advice regarding optical stimulation experiments. We thank The University of Chicago Materials Research Science and Engineering Centers, The University of Chicago Searle Cleanroom, and Argonne National Laboratory Center for Nanoscale Materials for their facilities and advice regarding material characterization and fabrication. We also thank The University of Chicago Human Tissue Resource Center for cryosectioning heart tissue for our phototoxicity experiments. We additionally thank Dr. Margaret Gardel for her advice on the in vitro cardiomyocyte optical stimulation experiments. The work was supported by the Air Force Office of Scientific Research (AFOSR FA9550-18-1-0503) and the Office of Naval Research (ONR Young Investigator Program, N000141612530; Presidential Early Career Award for Scientists and Engineers, N000141612958). R.P. acknowledges support from the Paul and Daisy Soros Foundation, NIH F30AI138156-02 Fellowship, and the NIH Medical Scientist Training Program training Grant T32GM007281. B.T. also acknowledges NIH (1DP2NS101488) and Army Research Office (W911NF-18-1-0042). H.-G.P. acknowledges support from National Research Foundation of Korea (NRF) grants funded by the Korean government (Ministry of Science and ICT) (2018R1A3A3000666 and 2017R1A4A1015426).

1. Cingolani E, Goldhaber JI, Marbán E (2018) Next-generation pacemakers: From small devices to biological pacemakers. *Nat Rev Cardiol* 15:139–150.
2. Jenkins MW, et al. (2010) Optical pacing of the embryonic heart. *Nat Photonics* 4: 623–626.
3. Li N, et al. (2017) Redundant and diverse intranodal pacemakers and conduction pathways protect the human sinoatrial node from failure. *Sci Transl Med* 9:eaam5607.
4. Savchenko A, et al. (2018) Graphene biointerfaces for optical stimulation of cells. *Sci Adv* 4:eaat0351.
5. Gentemann L, et al. (2016) Modulation of cardiomyocyte activity using pulsed laser irradiated gold nanoparticles. *Biomed Opt Express* 8:177–192.
6. Smith NI, et al. (2008) A femtosecond laser pacemaker for heart muscle cells. *Opt Express* 16:8604–8616.
7. Liu Q, Frerck MJ, Holman HA, Jorgensen EM, Rabbitt RD (2014) Exciting cell membranes with a blustering heat shock. *Biophys J* 106:1570–1577.
8. Simmons CS, Petzold BC, Pruitt BL (2012) Microsystems for biomimetic stimulation of cardiac cells. *Lab Chip* 12:3235–3248.
9. Nussinovitch U, Gepstein L (2015) Optogenetics for in vivo cardiac pacing and resynchronization therapies. *Nat Biotechnol* 33:750–754.
10. Roche ET, et al. (2017) Soft robotic sleeve supports heart function. *Sci Transl Med* 9: eaaf3925.

11. Jenkins MW, et al. (2013) Optical pacing of the adult rabbit heart. *Biomed Opt Express* 4:1626–1635.
12. Parameswaran R, et al. (2018) Photoelectrochemical modulation of neuronal activity with free-standing coaxial silicon nanowires. *Nat Nanotechnol* 13: 260–266.
13. Katz LC, Dalva MB (1994) Scanning laser photostimulation: A new approach for analyzing brain circuits. *J Neurosci Methods* 54:205–218.
14. Greytak AB, Barrelet CJ, Li Y, Lieber CM (2005) Semiconductor nanowire laser and nanowire waveguide electro-optic modulators. *Appl Phys Lett* 87:151103.
15. Park HG, et al. (2008) A wavelength-selective photonic-crystal waveguide coupled to a nanowire light source. *Nat Photonics* 2:622–626.
16. Sirbuly DJ, et al. (2005) Optical routing and sensing with nanowire assemblies. *Proc Natl Acad Sci USA* 102:7800–7805.
17. Jiang Y, et al. (2016) Heterogeneous silicon mesostructures for lipid-supported bioelectric interfaces. *Nat Mater* 15:1023–1030.
18. Jiang YW, et al. (2018) Rational design of silicon structures for optically controlled multiscale biointerfaces. *Nat Biomed Eng* 2:508–521.
19. Carvalho-de-Souza JL, Pinto BI, Pepperberg DR, Bezanilla F (2018) Optocapacitive generation of action potentials by microsecond laser pulses of nanojoule energy. *Biophys J* 114:283–288.
20. Chen R, Romero G, Christiansen MG, Mohr A, Anikeeva P (2015) Wireless magnetothermal deep brain stimulation. *Science* 347:1477–1480.
21. Chen S, et al. (2018) Near-infrared deep brain stimulation via upconversion nanoparticle-mediated optogenetics. *Science* 359:679–684.
22. Ghezzi D, et al. (2011) A hybrid bioorganic interface for neuronal photoactivation. *Nat Commun* 2:166.
23. Kim TI, et al. (2013) Injectable, cellular-scale optoelectronics with applications for wireless optogenetics. *Science* 340:211–216.
24. Minev IR, et al. (2015) Biomaterials. Electronic dura mater for long-term multimodal neural interfaces. *Science* 347:159–163.
25. Uhlén P (2004) Spectral analysis of calcium oscillations. *Sci STKE* 2004:pl15.